

**Intermediate-energy Coulomb excitation of  $^{104}\text{Sn}$ :  
Moderate  $E2$  strength decrease approaching  $^{100}\text{Sn}$**

P. Doornenbal,<sup>1,\*</sup> S. Takeuchi,<sup>1</sup> N. Aoi,<sup>2</sup> M. Matsushita,<sup>3,4</sup> A. Obertelli,<sup>5</sup>  
D. Steppenbeck,<sup>3</sup> H. Wang,<sup>1,6</sup> L. Audirac,<sup>5</sup> H. Baba,<sup>1</sup> P. Bednarczyk,<sup>7</sup> S. Boissinot,<sup>5</sup>  
M. Ciemala,<sup>7</sup> A. Corsi,<sup>5</sup> T. Furumoto,<sup>8</sup> T. Isobe,<sup>1</sup> A. Jungclaus,<sup>9</sup> V. Lapoux,<sup>5</sup>  
J. Lee,<sup>1</sup> K. Matsui,<sup>10</sup> T. Motobayashi,<sup>1</sup> D. Nishimura,<sup>11</sup> S. Ota,<sup>3</sup> E.C. Pollacco,<sup>5</sup>  
H. Sakurai,<sup>1,10</sup> C. Santamaria,<sup>5</sup> Y. Shiga,<sup>4</sup> D. Sohler,<sup>12</sup> and R. Taniuchi<sup>10</sup>

<sup>1</sup>*RIKEN Nishina Center, Wako, Saitama 351-0198, Japan*

<sup>2</sup>*Research Center for Nuclear Physics, Osaka University, Ibaraki, Osaka 567-0047, Japan*

<sup>3</sup>*Center for Nuclear Study, The University of Tokyo,  
RIKEN Campus, Wako, Saitama 351-0198, Japan*

<sup>4</sup>*Department of Physics, Rikkyo University, Toshima, Tokyo 172-8501, Japan*

<sup>5</sup>*CEA Saclay, Service de Physique Nucléaire, F-91191 Gif-sur-Yvette, France*

<sup>6</sup>*State Key Laboratory of Nuclear Physics and  
Technology, Peking University, Beijing 100871, P.R.China*

<sup>7</sup>*The Niewodniczanski Institute of Nuclear Physics,  
Polish Academy of Sciences, 31-342 Krakow, Poland*

<sup>8</sup>*Ichinoseki National College of Technology, Ichinoseki-shi 021-8511, Japan*

<sup>9</sup>*Instituto de Estructura de la Materia, CSIC, E-28006 Madrid, Spain*

<sup>10</sup>*Department of Physics, University of Tokyo, Bunkyo, Tokyo 113-0033, Japan*

<sup>11</sup>*Department of Physics, Tokyo University of Science, Noda, Chiba 278-8510, Japan*

<sup>12</sup>*Institute for Nuclear Research of the Hungarian  
Academy of Sciences, Debrecen, H-4001, Hungary*

(Dated: October 31, 2018)

## Abstract

The reduced transition probability  $B(E2)\uparrow$  of the first excited  $2^+$  state in the nucleus  $^{104}\text{Sn}$  was measured via Coulomb excitation in inverse kinematics at intermediate energies. A value of  $0.163(26) e^2\text{b}^2$  was extracted from the absolute cross-section on a Pb target, while the method itself was verified with the stable  $^{112}\text{Sn}$  isotope. Our result deviates significantly from the earlier reported value of  $0.10(4) e^2\text{b}^2$  and corresponds to a moderate decrease of excitation strength relative to the almost constant values observed in the proton-rich, even- $A$   $^{106-114}\text{Sn}$  isotopes. Present state-of-the-art shell-model predictions, which include proton and neutron excitations across the  $N = Z = 50$  shell closures as well as standard polarization charges, underestimate the experimental findings.

PACS numbers: 21.60.Cs,23.20.Js,25.70.DE

Across the Segré chart of nuclei the tin isotopes take an eminent position. Besides containing the longest chain of isotopes in-between two doubly-magic nuclei, in this case  $^{100}\text{Sn}$  and  $^{132}\text{Sn}$ , accessible to nuclear structure research, the valley of stability against  $\beta$ -decay crosses this chain at mid-shell. This allows for systematic studies of basic nuclear properties from very proton-rich  $N = Z$  to very neutron-rich nuclei. Of high interest in this context is the robustness of the proton  $Z = 50$  shell closure when the  $N = 50, 82$  magic numbers are approached. Experimentally, the  $Z = 50$  correlated gap size can be inferred from mass measurements when data from neighboring isotones is available. The magnitude of the proton gap is well known for neutron-rich nuclei beyond the end of the major shell and shows a maximum for  $^{132}\text{Sn}$  [1]. On the proton-rich side, however, experimental information is more scarce and only indirect evidence for a good  $Z = 50$  shell closure exists, e.g., the large Gamov-Teller strength observed in the  $\beta$  decay of  $^{100}\text{Sn}$  [2].

Complementary shell evolution probes can be obtained from the  $2_1^+ \rightarrow 0_{\text{g.s.}}^+$  transition energies,  $E(2_1^+)$ , and their reduced transition probabilities  $B(E2; 0_{\text{g.s.}}^+ \rightarrow 2_1^+)$ , in short  $B(E2)\uparrow$ . While the  $E(2_1^+)$  values of the tin isotopes between  $^{100}\text{Sn}$  and  $^{132}\text{Sn}$  are well established and exhibit only very little variation – the highest value is 1.472 MeV for  $^{102}\text{Sn}$ , the lowest is 1.132 MeV for  $^{124}\text{Sn}$  [3, 4] – the  $B(E2)\uparrow$  transition strengths follow a different pattern. The a priori expectation is a curve showing maximum collectivity at mid-shell and smoothly decreasing towards the shell closures, reflecting the number of particles times the number of holes available within the major shell. This perception is put on a formal base for a single  $j$ -shell by the seniority scheme (see, e.g., Ref. [5]), which predicts constant  $E(2_1^+)$  excitation energies and a parabolic pattern for the transition strengths. It has been shown that these key characteristics remain valid in the generalized seniority scheme as long as the orbits within the major shell are filled with the same rate, while for different level occupancies a shallow minimum for the  $B(E2)\uparrow$  values can be obtained at mid-shell [6].

In recent years, several experimental findings generated the large interest regarding the  $E2$  strengths pattern in the tin isotopes. While the neutron-rich isotopes with  $A = 126, 128, 130$  follow the anticipated trend of smoothly decreasing  $B(E2)\uparrow$  values towards the major shell closure [7, 8] well described by large-scale shell-model (LSSM) calculations [9, 10], the proton-rich nuclei take a different path. Commencing with the stable  $A = 114$  isotope a steadily growing deviation from the shell-model expectations was observed with almost constant  $B(E2)\uparrow$  values for the  $A = 106 - 112$  isotopes [9–14]. This triggered a revisit of the stable tin isotopes via direct lifetime measurements, yielding generally lower  $E2$  transition strengths than the adopted values given in

Ref. [4] and even a local minimum for the mid-shell  $A = 116$  nucleus [15].

While the  $B(E2)\uparrow$  value of  $^{102}\text{Sn}$  remains missing for a complete pattern of the tin isotopes within the major shell, a first attempt for  $^{104}\text{Sn}$  with limited statistics has recently been made [16]. The result of  $0.10(4) e^2b^2$  indicates a steep decrease of excitation strength in agreement with LSSM calculations. In order to ameliorate the experimental situation, a new measurement of the  $2_1^+$  transition strength in  $^{104}\text{Sn}$  is desirable. Here, we report on the first  $B(E2)\uparrow$  extraction in the unstable, proton-rich tin nuclei from absolute Coulomb excitation cross-sections. Previously deduced values relied on target excitation at “safe” [10, 11] and intermediate [12] energies or used a stable tin isotope with known excitation strength as normalization [9, 16]. In fact, all reported values from intermediate-energy Coulomb excitation measurements above 100 MeV/nucleon rely on the latter method [9, 17, 18] and so far no attempt has been made to determine absolute cross-sections at these high energies. Therefore, in the present work the stable  $^{112}\text{Sn}$  isotope, which has a known  $B(E2)\uparrow$  value, was Coulomb excited as well in order to validate the method.

The experiment was performed at the Radioactive Isotope Beam Factory (RIBF), operated by the RIKEN Nishina Center and the Center for Nuclear Study of the University of Tokyo. A  $^{124}\text{Xe}$  primary beam was accelerated up to an energy of 345 MeV/nucleon and impinged on a 3 mm thick Be production target at the F0 focus of the BigRIPS fragment separator [19]. The  $B\rho - \Delta E - B\rho$  method was applied to select and purify secondary beams of  $^{104}\text{Sn}$  and  $^{112}\text{Sn}$  in two subsequent measurements. The beam cocktail compositions were identified event-by-event. An ionization chamber located at the focal point F7 measured the energy loss  $\Delta E$ , yielding the fragments’ element number  $Z$ . The combination of position and angle measurements at the achromatic focal point F3 and the dispersive focal point F5 with parallel plate avalanche counters (PPAC) [20] and a time-of-flight (TOF) measurement with two plastic scintillators placed at the focal points F3 and F7 enabled the deduction of the mass-to-charge ratio  $A/Q$ . For the  $^{104,112}\text{Sn}$  secondary beams, momentum acceptances were 2.2% and 0.9%, respectively.

The secondary beams were transported to the focal point F8, where a 557 mg/cm<sup>2</sup> thick Pb target was inserted to induce Coulomb excitation reactions. At mid-target, the secondary beam energies were 131 and 154 MeV/nucleon for the  $^{104,112}\text{Sn}$  fragments. In order to enhance the number of tin fragments in the fully stripped charge state, a 6 mg/cm<sup>2</sup> thick aluminum foil was placed behind the reaction target. Scattering angles were determined with two PPACs located 1430 and 930 mm upstream and one PPAC located 890 mm downstream the secondary target. The PPACs’ position resolution in X and Y was 0.5 mm ( $\sigma$ ), allowing for a scattering angle

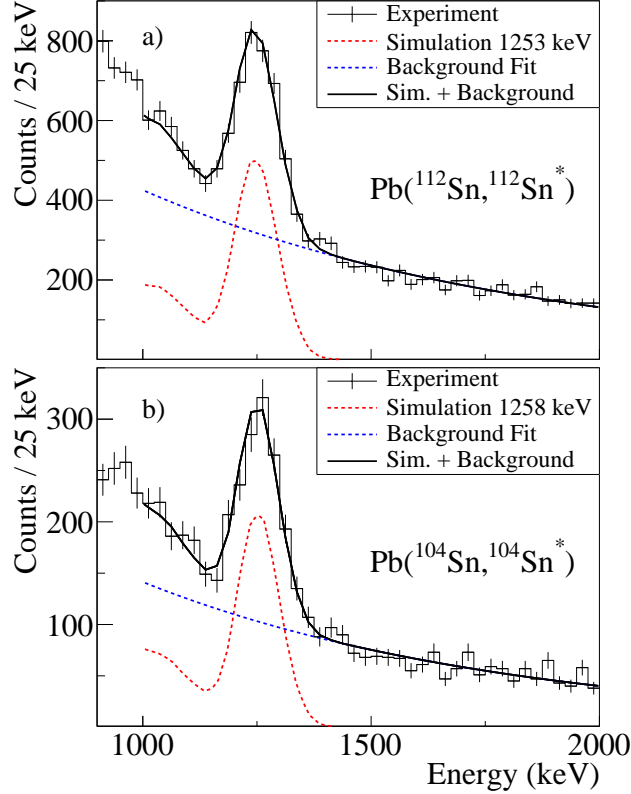


FIG. 1: (color online) Doppler corrected  $\gamma$ -ray energy spectra following Coulomb excitation of fully-stripped  $^{112}\text{Sn}$  (a) and  $^{104}\text{Sn}$  (b) ejectiles detected in coincidence with the BigRIPS and ZeroDegree spectrometers. Intensities were determined by fitting the observed line-shapes with simulated response functions (red dotted) on top of exponential background (blue dotted). The resulting curves are shown by the solid lines.

reconstruction resolution of about 5 mrad, while an angular straggling of 6–8 mrad was calculated with the ATIMA code [21]. Grazing angles, calculated using the formulas given in Ref. [22], were 28 and 23 mrad for  $^{104,112}\text{Sn}$  and their respective energies in front of the reaction target. Due to the scattering angle resolution and the angular straggling, a cut on “safe” angles would have led to a loss of a large fraction of the  $\gamma$ -ray yield. Therefore, no angular cut was applied and contributions from nuclear excitations were determined from inelastic scattering on a  $370 \text{ mg/cm}^2$  thick carbon target.

To detect  $\gamma$ -rays from the  $2_1^+ \rightarrow 0_{\text{gs}}^+$  transitions, the reaction target was surrounded by the DALI2 array [23]. It consisted of 186 NaI(Tl) detectors, covering center-of-crystal angles from 19 to 150 degrees. The efficiency of the DALI2 spectrometer was measured with  $^{60}\text{Co}$  and  $^{88}\text{Y}$  station-

ary sources and agreed within 5 % to simulations using GEANT4 [24]. For the 1.33 MeV  $\gamma$ -ray emitted by the stationary  $^{60}\text{Co}$  source, a full energy peak (FEP) detection efficiency of 14 % and an energy resolution of 6 % (FWHM) were measured for the full array. Radiation arising from secondary bremsstrahlung produced from the ions' deceleration in the reaction target was the anticipated main source of background. Therefore, the beam pipe at the F8 focus was enclosed by 1 mm of lead and 1 mm of tin shields. In addition, only forward angle detectors in the rest-frame were analyzed. After Doppler shift correction for a 1.26 MeV  $\gamma$ -ray emitted in-flight, values of 10 % and 8 % (FWHM) were expected for the FEP efficiency and energy resolution, respectively.

Reaction products behind the reaction target were identified by the ZeroDegree spectrometer [19], using the previously described  $\Delta E - B\rho$ -TOF method from focus F8 to focus F11. Angular acceptances were  $\pm 30$  mrad vertically and  $\pm 45$  mrad horizontally for particles passing ZeroDegree with the central momentum. Including efficiencies of 83 and 76 % for scattering angle determination, 180 and 920 particles per second of  $^{104,112}\text{Sn}$  ejectiles were detected in the ZeroDegree spectrometer in their fully-stripped charge state. Figure 1 displays the  $\gamma$ -ray spectra measured in coincidence with fully-stripped  $^{104,112}\text{Sn}$  ions detected in BigRIPS and ZeroDegree after applying the Doppler shift correction. The two transitions were observed at 1258(6) and 1253(6) keV, close to the literature values of 1260 and 1257 keV [4]. The intensities were determined by fitting the experimentally observed spectra with simulated response functions on top of exponential background.

The measured inelastic cross-sections  $\sigma_{2_1^+}$  are composed of contributions from nuclear excitation, Coulomb excitation to the  $2_1^+$  state, and Coulomb feeding from higher lying states ( $\sigma_{2_1^+} = \sigma_n + \sigma_c + \sigma_f$ ). In addition, the ZeroDegree angular acceptance depends on the momentum distribution of the secondary beam and has to be corrected for. Thus, a measured cross-section on the Pb target can be converted to a  $B(E2)\uparrow$  value only if  $\sigma_n$  and  $\sigma_f$  are quantified.

Inelastic scattering cross sections to the  $2_1^+$  state of 40(4) and 48(4) mbarn were measured for the  $^{104,112}\text{Sn}$  isotopes on the carbon target. These values were reproduced with the DWEIKO code [25] by selecting nuclear vibrational excitations and deformation lengths of  $\delta = 0.38(2)$  and 0.45(2) fm. Optical potentials were derived for the calculations as described in Ref. [26] using the microscopic folding model with the complex G-matrix interaction CEG07 [27, 28] and the density presented in Ref. [29].

For inelastic scattering of  $^{112}\text{Sn}$  on the Pb target, the cross-section to the  $2_1^+$  state was  $\sigma_{2_1^+} = 524(39)$  mbarn, while a cross-section of  $\sigma_n + \sigma_c = 412(13)$  mbarn was calculated with DWEIKO

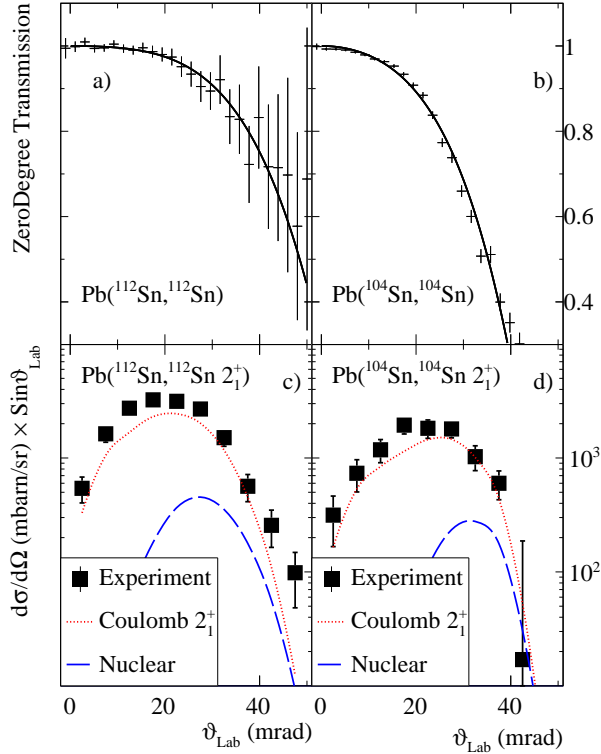


FIG. 2: (color online) The two top panels display the ZeroDegree transmission as function of the scattering angle for  $^{112}\text{Sn}$  (a) and  $^{104}\text{Sn}$  (b) on the Pb target, in the two bottom panels the differential inelastic scattering cross-sections are shown for  $^{112}\text{Sn}$  (c) and  $^{104}\text{Sn}$  (d). The calculated distributions are Coulomb excitation of the  $2_1^+$  state (red dotted) and the nuclear excitation (blue dashed). The difference between measured and the calculated cross-sections is attributed to Coulomb feeding from higher lying states. See text for details.

using the  $B(E2)\uparrow$  value of  $0.242(8) e^2b^2$  [4, 14], the derived deformation length, and the angular transmission shown in Fig. 2 (a). Thus, a Coulomb feeding contribution of  $\sigma_f = 112(41)$  mbarn was determined. Figure 2 (c) displays the measured differential cross-section as function of scattering angle. It is compared to the calculated nuclear cross-sections and to the  $2_1^+$  Coulomb excitation cross-section. Coulomb excitations are dominant for all scattering angles, as nuclear contributions are sizable only around the grazing angle. A larger nuclear contribution would have resulted in a maximum at the grazing angle. All calculations were convoluted with the detector resolution, the angular straggling, and the observed ZeroDegree scattering angle transmission.

The Coulomb feeding can be attributed to single-step Coulomb excitations to higher lying states and subsequent decay via the  $2_1^+$  state, while multi-step excitations play only a minor role at in-

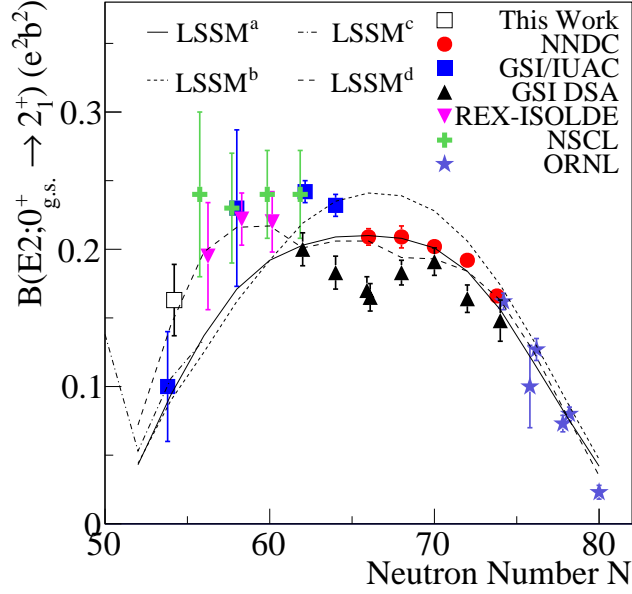


FIG. 3: (color online) Experimental  $B(E2)\uparrow$  values for even-mass Sn isotopes in-between the doubly magic  $^{100}\text{Sn}$  and  $^{132}\text{Sn}$  nuclei [4, 7–14]. Results from LSSM calculations using different inert cores and effective charges are shown for comparison. See text for details.

intermediate energies. For example, the  $B(E3)\uparrow$  value to the  $3_1^-$  state at 2355 keV in  $^{112}\text{Sn}$  has a strength of  $0.087(12) e^2 b^3$  [30] and decays through the  $2_1^+$  state. This translates to a feeding contribution of  $10(2)$  mbarn. For  $E2$  excitations, the total strength measured in the heavier  $^{116-124}\text{Sn}$  isotopes between two and four MeV corresponds to about 10 % of that to the first excited state [31], while no experimental information is available for  $2^+$  states at higher energies.

The observed Coulomb feeding contributions in  $^{112}\text{Sn}$  can be used to evaluate the Coulomb feeding for  $^{104}\text{Sn}$ . In a simple picture, it originates from the  $3_1^-$  excitation and fragmentation of the  $E2$  excitation strength to many  $2^+$  states between 2 MeV and the proton separation energy  $S_p$  (7.554(5) MeV for  $^{112}\text{Sn}$  and 4.286(11) MeV for  $^{104}\text{Sn}$  [1]). Assuming an uniform  $E2$  excitation strength distribution in this region, the same  $E3$  excitation strength and correcting for the angular transmission shown in Fig. 2 (b) results in a Coulomb feeding of  $\sigma_f = 46(19)$  mbarn for  $^{104}\text{Sn}$ , mainly due to the lower  $S_p$  value. This estimation is corroborated by a higher peak-to-background ratio for  $^{104}\text{Sn}$  despite a lower total cross-section, showing that fewer high lying excited states are populated.

For inelastic scattering of  $^{104}\text{Sn}$  on the Pb target, a cross section of  $\sigma_{2_1^+} = 298(30)$  mbarn was measured. Taking the previously determined nuclear contributions and the Coulomb feeding into



account, a  $B(E2)\uparrow$  of  $0.163(26) e^2b^2$  was deduced. Note that due to the lower beam energy and the reduced scattering angle acceptance, nuclear contributions were significantly suppressed ( $\sigma_n = 28(3)$  mbarn), as can be seen in the differential cross-section in Fig. 2 (d). The new  $B(E2)\uparrow$  value is displayed in Fig. 3 together with known data in-between the two doubly-magic tin nuclei. Our result deviates significantly from the value of  $0.10(4) e^2b^2$  obtained in Ref. [16]. It corresponds to only about 30 % excitation strength decrease compared to the even- $A$   $^{106-114}\text{Sn}$  isotopes and shows that the reduction is much more shallow than previously suggested.

Correlated with the recent experimental progress approaching  $^{100}\text{Sn}$ , various  $B(E2)\uparrow$  calculations have been presented [6, 9, 10, 16, 32, 33]. Very instructive are the LSSM calculations presented with the first intermediate-energy Coulomb excitation experiment on proton-rich tin isotopes [9]. Within that work, two sets of  $B(E2)\uparrow$  calculations were performed, using  $^{100}\text{Sn}$  and  $^{90}\text{Zr}$  as inert cores, respectively, and an effective interaction derived from the CD-Bonn potential [34]. The former, denoted LSSM<sup>a</sup>, used a neutron model space with the  $1d_{5/2}$ ,  $0g_{7/2}$ ,  $1d_{3/2}$ ,  $2s_{1/2}$ , and  $0h_{11/2}$  orbitals, the latter, denoted LSSM<sup>b</sup>, contained the proton  $0g_{9/2}$ ,  $0g_{7/2}$ ,  $1d_{5/2}$ ,  $1d_{3/2}$ , and  $2s_{1/2}$  ( $gds$ ) orbitals as well. Neutron effective charges of  $e_\nu = 1.0e$  were used for the  $^{100}\text{Sn}$  core calculations to compensate the neglect of proton excitations across the  $Z = 50$  shell while the  $^{90}\text{Zr}$  core calculations allowed up to four-particle-four-hole proton excitations and used “standard” neutron and proton effective charges of  $e_\nu = 0.5e$  and  $e_\pi = 1.5e$ . The results are added in Fig. 3 to the experimental values between the two doubly magic nuclei and yield inverted parabola in agreement with the neutron rich nuclei but fail to reproduce the  $B(E2)\uparrow$  enhancement for proton-rich nuclei.

In the most recent shell model prediction, denoted LSSM<sup>c</sup> in Fig. 3, the calculations were expanded to a  $^{80}\text{Zr}$  core and a  $gds$  model space, thereby allowing neutron as well as proton excitations across the  $N = Z = 50$  gap [16]. The standard effective charges were used and truncation was applied depending on the nuclei’s neutron number due to computational limits. However, the inclusion of neutron excitations across the  $N = 50$  gap augmented the  $B(E2)\uparrow$  values only slightly. For  $^{104}\text{Sn}$ , a value of about  $0.1 e^2b^2$  is predicted, well below our experimental finding, and also the experimental  $B(E2)\uparrow$  values for  $^{106}\text{Sn}$  are underestimated.

Different suggestions to break the symmetry in the theoretical  $B(E2)\uparrow$  pattern have been made ranging from refined tuning of the proton-neutron monopoles [9, 11], inclusion of excitation across the  $N = 50$  shell [9], a  $N = 50$  shell gap reduction [10], to simply using two different sets of single particle levels and effective charges for the lower and upper half of the shell [32]. In an alternative

approach that included the neutron  $gds$  and  $0h_{11/2}$  orbitals as model space and single-particle energies fitted to experimental data [35], isospin-dependent effective charges as proposed by Bohr and Mottelson [36] were introduced into the calculations [33]. The neglect of proton excitations was compensated by normalizing the effective charges to  $e_v = 1.0e$  in the middle of the shell for  $^{116}\text{Sn}$  resulting in  $e_v > 1.0e$  ( $e_v < 1.0e$ ) in the lower (upper) half of the shell. Indeed, a good overall agreement is observed for very neutron and proton rich nuclei, as shown in Fig. 3 by LSSM<sup>d</sup>. However, the collectivity increase on the proton-rich side commences later than observed in experiments [13–15] and the large effective charges are also coincident with the proton gap minimum around  $^{108}\text{Sn}$  (see, e.g., Fig. 4 of Ref. [13]).

In combination with the neglect of proton excitations, this effective charge adjustment can therefore only be regarded as an interim solution until sufficient computing power becomes available. The importance of proton excitations across the  $Z = 50$  shell for a correct description of the  $B(E2)\uparrow$  pattern can be easily inferred from the difference in “matter” deformation lengths obtained from the carbon target and the charge deformation lengths obtained from the  $B(E2)\uparrow$  values. With  $\delta_c = (4\pi/3eZR_0)B(E2)\uparrow^{1/2}$  and  $R_0 = 1.2A^{1/3}$  fm, the latter are  $\delta_c = 0.59(9)$  and  $0.71(2)$  fm for  $^{104,112}\text{Sn}$  and hence about 50 % larger than the values of  $\delta = 0.38(2)$  and  $0.45(2)$  fm obtained with the carbon target.

In summary, a  $B(E2)\uparrow$  value of  $0.163(26) e^2b^2$  was measured for  $^{104}\text{Sn}$  in intermediate-energy Coulomb excitation. The drop in excitation strength is much smoother than obtained in [16] and cannot be reproduced by present LSSM calculations using standard effective charges as well as proton and neutron excitation across the  $N = Z = 50$  shell. Moreover, it was demonstrated that given the significant scattering angle resolution and angular straggling at energies well above 100 MeV/nucleon, nuclear excitation should be explicitly taken into account in  $B(E2)\uparrow$  determinations rather than suppressed in an inaccurate angular cut. Coulomb feeding from higher lying states cannot be neglected but can easily be determined from known  $B(E2)\uparrow$  values. A simple scaling of measured cross-sections for the  $^{104,112}\text{Sn}$  pair would have led to a 10 % lower  $B(E2)\uparrow$  assignment for  $^{104}\text{Sn}$ . Therefore, we suggest that future absolute cross-section measurements at energies well above 100 MeV/nucleon include calibration runs of nuclei with known  $B(E2)\uparrow$  values on a high  $Z$  target and nuclear excitation on a low  $Z$  target. Such an approach allows for the use of very thick reaction targets and thus gives access to more exotic nuclei.

We would like to thank the RIKEN Nishina Center Accelerator Division for providing the high  $^{124}\text{Xe}$  primary beam intensity and the BigRIPS team for preparing secondary beams with high

purities for the isotopes of interest. We acknowledge financial support from the Spanish Ministerio de Ciencia e Innovación under contracts FPA2009-13377-C02-02 and FPA2011-29854-C04-01, the OTKA under contract number K100835, and the European Research Council through the ERC Starting Grant MINOS-258567.

---

\* Electronic address: pieter@ribf.riken.jp

- [1] M. Wang, G. Audi, A. Wapstra, F. Kondev, M. MacCormick, X. Xu, and B. Pfeiffer, *Chin. Phys. C* **36**, 1603 (2012).
- [2] C. Hinke et al., *Nature* **486**, 341 (2012).
- [3] M. Lipoglavsek et al., *Z. Phys. A* **356**, 239 (1996).
- [4] S. Raman, C. W. N. Jr., and P. Tikkanen, *Atom. Data and Nucl. Data Tab.* **78**, 1 (2001).
- [5] R. Casten, *Nuclear Structure from a Simple Perspective* (Oxford University Press, 2001).
- [6] I. Morales, P. V. Isacker, and I. Talmi, *Phys. Lett. B* **703**, 606 (2011).
- [7] D. Radford et al., *Nucl. Phys. A* **746**, 83c (2004).
- [8] J. Allmond et al., *Phys. Rev. C* **84**, 061303(R) (2011).
- [9] A. Banu et al., *Phys. Rev. C* **72**, 061305 (2005).
- [10] A. Ekström et al., *Phys. Rev. Lett.* **101**, 012502 (2008).
- [11] J. Cederkäll et al., *Phys. Rev. Lett.* **98**, 172501 (2007).
- [12] C. Vaman et al., *Phys. Rev. Lett.* **99**, 162501 (2007).
- [13] P. Doornenbal et al., *Phys. Rev. C* **78**, 031303 (2008).
- [14] R. Kumar et al., *Phys. Rev. C* **81**, 024306 (2010).
- [15] A. Jungclaus et al., *Phys. Lett. B* **110**, 695 (2011).
- [16] G. Guastalla et al., *Phys. Rev. Lett.* **110**, 172501 (2013).
- [17] A. Bürger et al., *Phys. Lett. B* **622**, 29 (2005).
- [18] T. Saito et al., *Phys. Lett. B* **669**, 19 (2008).
- [19] T. Kubo et al., *Prog. Theor. Exp. Phys.* **2012**, 03C003 (2012).
- [20] H. Kumagai, A. Ozawa, N. Fukuda, K. Sümmerer, and I. Tanihata, *Nucl. Instrum. and Meth. A* **470**, 562 (2001).
- [21] *Atima*, <http://web-docs.gsi.de/~weick/atima/>.
- [22] H. Wollersheim et al., *Nucl. Instrum. and Meth. A* **537**, 637 (2005).

- [23] S. Takeuchi et al., in *RIKEN Accelerator Progress Report* (RIKEN, 2003), vol. 36, p. 148.
- [24] S. Agostinelli et al., *Nucl. Instr. Meth. A* **506**, 250 (2003).
- [25] C. A. Bertulani, C. M. Campbell, and T. Glasmacher, *Comp. Phys. Com.* **152**, 317 (2003).
- [26] T. Furumoto, W.Horiuchi, M.Takashina, Y.Yamamoto, and Y.Sakuragi, *Phys. Rev. C* **85**, 044607 (2012).
- [27] T. Furumoto, Y. Sakuragi, and Y. Yamamoto, *Phys. Rev. C* **78**, 044610 (2008).
- [28] T. Furumoto, Y. Sakuragi, and Y. Yamamoto, *Phys. Rev. C* **80**, 044614 (2009).
- [29] L. Chamon et al., *Phys. Rev. C* **66**, 014610 (2002).
- [30] N. Jonsson, A. Backlin, J. Kantele, R. Julin, M. Luontama, and A. Passoja, *Nuclear Physics A* **371**, 333 (1981).
- [31] A. Bryssinck et al., *Phys. Rev. C* **61**, 024309 (2000).
- [32] H. Jiang, Y. Lei, G. Fu, Y. Zhao, and A. Arima, *Phys. Rev. C* **86**, 054304 (2012).
- [33] T. Bäck, C. Qi, B. Cederwall, R. Liotta, F. G. Moradi, A. Johnson, R. Wyss, and R. Wadsworth, *Phys. Rev. C* **87**, 031306(R) (2013).
- [34] R. Machleidt, *Phys. Rev. C* **63**, 024001 (2001).
- [35] C. Qi and Z. Xu, *Phys. Rev. C* **86**, 044323 (2012).
- [36] A. Bohr and B.Mottelson, *Nuclear Structure, Vol. II* (Benjamin, New York, 1975).